Environmental Science & Technology

pubs.acs.org/est

Article

Influence of Organic Ligands on the Redox Properties of Fe(II) as Determined by Mediated Electrochemical Oxidation

Jeffrey M. Hudson,* George W. Luther, III, and Yu-Ping Chin*

Cite This: *Environ. Sci. Technol.* 2022, 56, 9123−9132

Read Online

ACCESS | Metrics & More | Article Recommendations | Supporting Information

ABSTRACT: Fe(II) has been extensively studied due to its importance as a reductant in biogeochemical processes and contaminant attenuation. Previous studies have shown that ligands can alter aqueous Fe(II) redox reactivity but their data interpretation is constrained by the use of probe compounds. Here, we employed mediated electrochemical oxidation (MEO) as an approach to directly quantify the extent of Fe(II) oxidation in the absence and presence of three model organic ligands (citrate, nitrilotriacetic acid, and ferrozine) across a range of potentials (E_H) and pH, thereby manipulating oxidation over a broad range of fixed thermodynamic conditions. Fe(III)-stabilizing ligands enhanced Fe(II) reactivity in thermodynamically unfavorable regions (i.e., low pH and E_H) while an Fe(II) stabilizing ligand (ferrozine) prevented oxidation across all thermodynamic regions. We experimentally derived apparent standard redox potentials, E_H^ϕ, for these and other (oxalate, oxalate$_2$, NTA$_2$, EDTA, and OH$_2$) Fe-ligand redox couples via oxidative current integration. Preferential stabilization of Fe(III) over Fe(II) decreased E_H^ϕ values, and a Nernstian correlation between E_H^ϕ and $\log(K_{Fe(III)}/K_{Fe(II)})$ exists across a wide range of potentials and stability constants. We used this correlation to estimate $\log(K_{Fe(III)}/K_{Fe(II)})$ for a natural organic matter isolate, demonstrating that MEO can be used to measure iron stability constant ratios for unknown ligands.

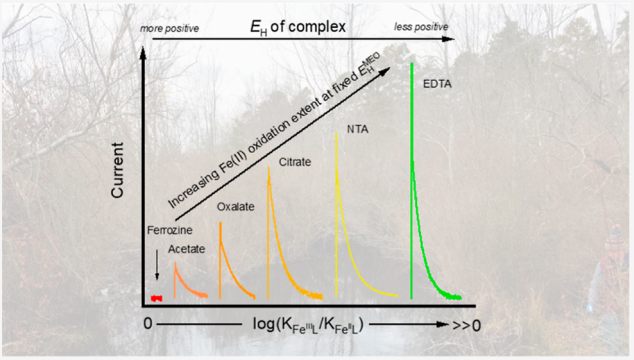

KEYWORDS: *ligand, redox potential, stability constant, MEO, ferrozine, Fe(II)*

INTRODUCTION

Iron is one of the most abundant elements in earth's crust and exists primarily in (+II) and (+III) oxidation states in environmental compartments.[1] Under oxic conditions, Fe(III) predominates over Fe(II) in the form of poorly soluble or insoluble iron-oxyhydroxides,[2,3] while Fe(II) predominates in anoxic or low pH environments.[3,4] Aqueous, sorbed, and solid-phase Fe(II) has been extensively studied due to its importance as a reductant in biogeochemical processes and contaminant attenuation.[5−7] Growing attention has been specifically paid to Fe(II) complexes (Fe^{II}−L), as complexation of Fe(II) by ubiquitous natural organic matter in the environment is prevalent and expected at most redox interfaces including soils, sediment porewaters, and water column redoxclines.[8−11]

Both inorganic and organic ligands (L) have been shown to alter the redox reactivity of Fe(II).[5,12−14] Soluble Fe(II)-organic complexes, such as those present in dissolved organic matter (DOM), can alter the reactivity of Fe(II) as a reductant.[5,13,15,16] Organic ligands that preferentially stabilize Fe(III) as opposed to Fe(II) decrease its standard state electron reduction potential (E_H^0) and can increase its ability to reduce inorganic and organic contaminants, e.g., chromium,[15] nitroaromatics,[17,18] and pesticides.[14] The decrease in E_H^0 of the $Fe^{III}L/Fe^{II}L$ redox couple is caused by the larger thermodynamic stability constants for Fe(III) relative to Fe(II) (i.e., $\log K_{Fe(III)} > \log K_{Fe(II)}$) (eq 1).[17,18]

$$E_H^0 = 0.77 - 0.059 \log\left(\frac{K_{Fe(III)L}}{K_{Fe(II)L}}\right) \quad (1)$$

Fe(III)-stabilizing ligands induce a high spin iron electron configuration[19,20] and are typically comprised of low molecular weight acids, which include functional groups rich in oxygen, (carboxylates, catecholates, hydroxymates, and phenolates),[17,21−27] sulfur (cysteine, thiol),[18,28−30] and nitrogen (porphyrins).[31] Some strong ligands, such as nitrilotriacetic acid (NTA) and ethylenediaminetetraacetic acid (EDTA) have both oxygen and nitrogen components.[19,32,33] Fe(II)-stabilizing ligands, such as ferrozine and phenanthroline, are known to have bipyridyl moieties in their structure and contain only N

Received: March 14, 2022
Revised: May 14, 2022
Accepted: May 16, 2022
Published: June 8, 2022

https://doi.org/10.1021/acs.est.2c01782
Environ. Sci. Technol. 2022, 56, 9123−9132

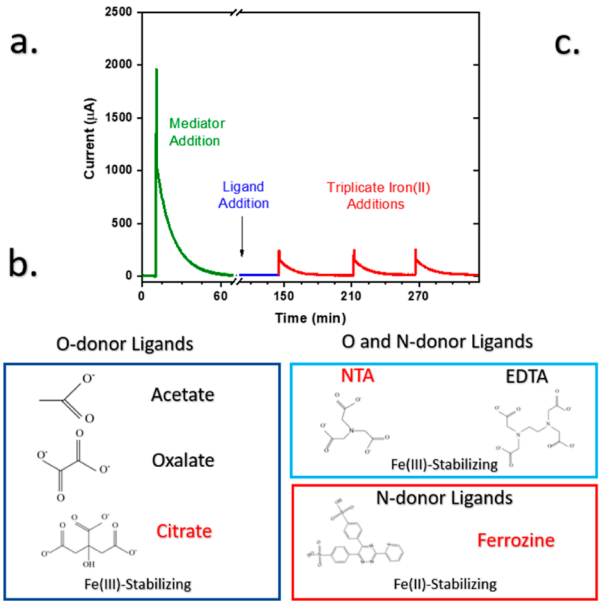

c.

Fe(II) species	E_H^0	Coordination Positions
Fe^{2+}	0.77	0
$FeOH^+$	0.34	1
$Fe(OH)_2$	-0.10	2
$FeCl^+$	0.68	1
$Fe(Acetate)^+$	0.63	1-2
Fe(Oxalate)	0.50	2
$Fe(Oxalate)_2^{2-}$	0.25	4
$Fe(Oxalate)_3^{4-}$	-0.02	6
$Fe(Citrate)^-$	0.37	3
FeH(Citrate)	0.53	3
$Fe(NTA)^-$	0.36	4
$Fe(NTA)_2^{4-}$	0.06	6
$Fe(OH)(NTA)^{2-}$	n.a.	5
$Fe(EDTA)^{2-}$	0.13	6
$Fe(Ferrozine)_3$	0.97*	6

Figure 1. Overview of experimental spiking scheme and ligands chosen for Fe(II) oxidation experiments. (a) Experimental spiking scheme for MEO experiments. Green represents the addition of a mediator, while blue and red colors represent ligand addition and triplicate iron additions to the cell, respectively. Ligands were not electroactive resulting in a lack of current response upon addition to the cell. (b) Structures of organic ligands used in our study, divided by both ligand atom-donor properties, as well as the ligands Fe(III)- or Fe(II)-stabilizing properties. Ligands used to profile the extent of Fe(II) oxidation across E_H and pH conditions are highlighted in red. (c) Previously reported standard one-electron reduction potentials and coordination positions of some common Fe(II) complexing ligands that are present in our study. The asterisk by ferrozine denotes the value we obtained using mediated potentiometry (Supporting Information Section S9).

ligating atoms and induce low spin iron.[19,34,35] Recent studies have either modeled or experimentally determined that the majority of Fe(II) complexed to DOM binds to carboxylate and phenolate groups due to their abundance in DOM. Conversely, while sulfur and nitrogen containing ligands are stronger, they are much less abundant in DOM.[21,22]

While results from previous studies have shown how organic complexation can alter the abiotic and biotic reactivity of Fe(II) as a reductant,[5,13−18,26−28,36,37] the effects of complexation on the oxidation of Fe(II) remain unclear. Most studies employ probe compounds, which link calculated metal−ligand stability constants (and henceforth, E_H) to experimentally derived, compound specific reduction kinetics to produce linear free-energy relationships.[13−15,17,18] Kinetics indicate reactivity, but often times, redox kinetics do not match expected rates calculated from linear free energy relationships due to the nature of the electron transfer (i.e., inner vs. outer sphere).[13,14,26] Furthermore, probe experiments are limited in their ability to profile Fe(II) oxidation over a range of oxidizing potentials because these compounds have a single, fixed potential.[13,14,14,15,18,38] Limiting the experimental potential range over which Fe(II) oxidation can occur constrains our ability to holistically interpret the redox reactivity of Fe(II) in the environment.[4,13,39,40]

For our study, we applied mediated electrochemical analysis (MEA) to directly investigate and compare the effect of model organic ligands on Fe(II) redox properties. This approach has been previously used to study the reactivity of humic substances and mineral phases,[41−44] and redox reactions can be controlled under highly constrained thermodynamic conditions (i.e., fixed E_H and pH) inside the electrochemical cell.[45] Specifically, we used mediated electrochemical oxidation (MEO) to study Fe(II) oxidation in the absence and presence of two model organic Fe(III) stabilizing ligands, citrate and NTA, as well as one model Fe(II) stabilizing ligand, ferrozine, across a range of oxidizing E_H and pH, which can be controlled by the applied potential to the cell and the buffered conditions within the cell, respectively. In MEO, a reduced species undergoes oxidation within the cell in the presence of a mediating compound[44] and its ability to donate electrons is quantified by integrating the oxidative current peaks.[43,44] To the best of our knowledge, this is the first study that provides direct experimental evidence on how organic ligands alter the redox properties of Fe(II) under different E_H and pH conditions. We believe our work complements previous Fe(III) reduction work by Aeppli et al. as we complete the investigation of Fe redox transformations across the E_H-pH stability region.[45] Following our profiling work with citrate, NTA, and ferrozine, we used Fe^{III}/Fe^{II} ratios obtained via current peak integration[44,46,47] [i.e., number of electrons transferred from Fe(II) to Fe(III)] to determine apparent reduction potentials, $E_H\Phi$,[44,46,47] of other model organic iron-ligand complexes in the electrochemical cell. Redox potentials measured via MEO formed a linear, Nernstian relationship when plotted versus known thermodynamic stability constants and allowed us to estimate unknown iron-DOM stability constants for Suwannee River Natural Organic Matter (SRNOM).

MATERIALS AND METHODS

Chemicals. A complete list of chemicals used in our experimental work can be found in the Supporting Information (SI Section S1).

Solutions. Solutions were prepared from deionized water and deoxygenated by purging with argon (99.9% purity) on a heat plate at 100 °C. All MEO experiments, as well as cyclic voltammetry experiments, were performed in aqueous solutions containing pH buffers [all 0.01 M; acetic acid for

https://doi.org/10.1021/acs.est.2c01782
Environ. Sci. Technol. 2022, 56, 9123−9132

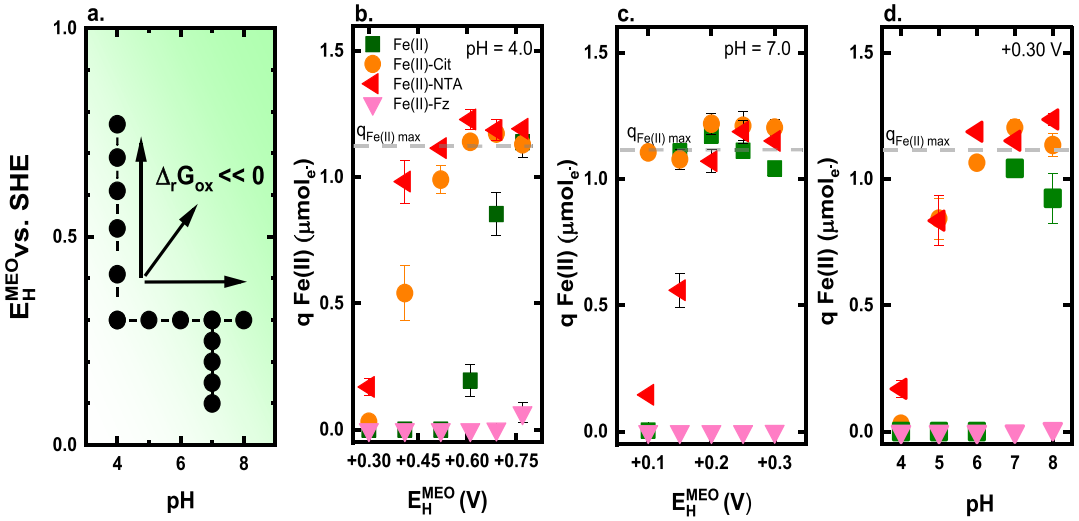

Figure 2. (a) Overview of experiments. Darker green areas in panel 1 represent experiments where peak response ($q_{Fe(II)}$) was generated. $q_{Fe(II)}$ in Fe(II) -alone, citrate, and NTA experiments increased at higher $E_H^{MEO}$and pH due to a more favorable Gibbs free energy of oxidation ($\Delta_r G_{ox}$, denoted by arrows) that is caused by applying a higher E_H^{MEO} to the electrode or by a decrease in the reduction potential of the iron redox couple and introduction of ligating hydroxide species at higher pH. (b) $q_{Fe(II)}$ versus E_H^{MEO} at pH 4. Note that $q_{Fe(II)max}$ (gray dashed line) refers to the maximum number of electrons expected to be donated from the total number of Fe(II) atoms [i.e., if every mol of Fe(II) was oxidized to Fe(III)]. Fe(II) (donated by the green symbol) represents scenarios where Fe(II) is added to the cell in the absence of an organic ligand. (c) $q_{Fe(II)}$ versus E_H^{MEO} at pH 7. (d) $q_{Fe(II)}$ versus pH at E_H^{MEO} +0.3 V. All experiments were performed with a ligand-to-Fe(II) molar ratio of 10:1.

pH 4 and 5; 2-(*N*-morpholino) ethanesulfonic acid (MES) for pH 6, 2-[4-(2-hydroxyethyl)piperazin-1-yl]-ethanesulfonic acid for pH 7 and 8, and CHES for pH 9] in a background electrolyte of 0.1 M KCl.

Mediated Electrochemical Oxidation. MEO of Fe^{II} in the presence and absence of organic ligands was performed using well-established chronoamperometric methods.[42,44−47] Electrochemical experiments were performed inside an anoxic, N_2-atmosphere glovebox (Plas Labs, Lansing, MI) (95% N/5% H). We used electrochemical cells comprised of 40 mL glassy carbon cylinders (GAZ 4, HTW Germany), which served both as the reaction vessel and working electrode (WE). The solution in each WE cylinder was stirred continuously with a Teflon-coated stir bar. Potential (E_H^{MEO}) measurements were determined against Ag/AgCl reference electrodes (BASi) and are corrected to the standard hydrogen electrode (SHE) and reported as such hereafter. Each cell contained a platinum wire counter electrode (BASi) that was separated from the WE compartment by a porous glass frit (PORE E tubes; ACE glass). The cells were controlled by Bluetooth-enabled potentiostats (Dropsens, Metrohm). Current data were collected with a 4 s sampling frequency.

The extent of Fe(II) oxidation was profiled (triplicate experiments) in the absence and presence of citrate, NTA, and Ferrozine at fixed E_H^{MEO} and solution pH. We chose these ligands to profile Fe(II) oxidation, as they can bind Fe^{II} across a wide range of pH values (i.e., they have low pK_a values), contain a different number of ligands that occupy a range of Fe(II) octahedral coordination positions (2−6), have different ligand donor atoms (oxygen and nitrogen donors), and represent both Fe(III)- and Fe(II)-stabilizing complexes (Figure 1).[13,15] In addition to citrate, NTA, and ferrozine, we added oxalate, EDTA, and SRNOM as ligands for the experimental determination of iron-ligand redox potentials (see below) to complement our profiling work and provide more variation in ligand binding modes. Further, at pH 4 and 5, our acetate buffer also acted as a very weak ligand for Fe(II).

After filling the WE cylinder and counter electrode compartment with 32 and 4 mL, respectively, of one of the pH-buffered solutions, experiments were initiated by applying a constant E_H^{MEO} to the WE. After the background current in the cell decreased and stabilized to values close to 0 μA, an electron transfer mediator was spiked into the WE cell (Figure 1a). We investigated five mediators (Figure S1) and chose 4 (2,2′-azinobis(3-ethylbenzthiazoline-6-sulfonic acid) diammonium salt, hydroquinone, 2,6-dichlorophenol-indophenol, and hexaammineruthenium(II) chloride (Ru), to cover our range of experimental E_H^{MEO} (+0.3 to +0.77 V at pH 4, +0.1 to +0.3 V at pH 7; Figure 2a). The choice of mediator reflected both the E_H^{MEO} controlled by the cell and other factors discussed elsewhere (Supporting Information Section S2.1, S2.2, and S2.3). Total mediator concentrations within the cell (300−450 μM) in all experiments were always in excess of the total Fe(II) to be added into the cell and were effective at facilitating electron transfer in our experiments (Supporting Information Section S2.4). Following addition of the mediators, the target organic ligand was spiked directly into the cell (Figure 1a). For profiling work across multiple E_H^{MEO} and pH, the ligand concentration in the cell was selected to be 10 times (∼300 μM) in excess of the initial Fe^{II} to be spiked into the cell (∼30 μM) in order to ensure complete complexation of Fe(II). In other speciation experiments, added ligand concentrations were adjusted to experimentally determine reduction potentials of both mono and bis complexes (Supporting Information Sections S3 and S4). Apart from SRNOM, all model ligands added to the cell were not electroactive, resulting in no change of current (Figure 1a). Fe(II) was added to the cell in three triplicate spikes following ligand addition to the cell. The reduction of the oxidized mediator by Fe(II) caused a current response that was a result of the change in the ratio of the oxidized to reduced mediator within the cell. The current response was analyzed for the number of electrons donated by Fe(II), $q_{(Fe^{II})}$, and represents the extent of Fe(II) oxidized at a fixed E_H^{MEO} and pH.

https://doi.org/10.1021/acs.est.2c01782
Environ. Sci. Technol. 2022, 56, 9123−9132

Data Analysis. The extent of Fe(II) oxidation, $q_{(Fe^{II})}$ [mol e^-], was quantified as the number of electrons transferred from Fe(II) as it was oxidized to Fe(III) (on a per mass basis) and was calculated by integrating the area underneath the current peak and is represented by eq 2

$$q_{(Fe^{II})} = \frac{1}{F}\int_{t_0}^{t_{end}} I(t)dt \quad (2)$$

where $I(t)$ is the baseline-corrected oxidative current in amperes (A), F is the Faraday constant (96,485 J/mol), and t_0 and t_{end} are the initial and final integration boundaries of the individual current peak (in seconds). Integration was performed using the peak analyzer tool in Origin 2019. Because our $FeCl_2$ stock solution concentrations were approximately 10 mM, injecting 110 μL of $FeCl_2$ into the cell resulted in a total mass and $q_{(Fe^{II}max)}$ that equaled 1.1 μmoles of electrons if every mole of Fe(II) was oxidized to Fe(III). For profiling experiments across multiple E_H^{MEO} and pH, triplicate experiments of Fe(II) oxidation peaks were all analyzed and averaged for $q_{(Fe^{II})}$.

Thermodynamic Calculations and Modeling. Known stability constants from the literature were checked using the Visual MINTEQ database under our solution conditions (Supporting Information Sections S5−S7). From these values, redox potentials for iron ligand (FeL) complexes were calculated using the Nernst equation (Supporting Information Section S8). For ferrozine, we measured the redox potential of the FeL_3 complex using potentiometry as it has never been reported (Supporting Information Section S9). This potential was used to calculate the thermodynamic and conditional constant for the Fe^{III}−L_3 complex as the conditional constant for the Fe^{II}−L_3 complex is known (Supporting Information Section S10, Tables S3 and S4).[34] We determined reduction potentials for Fe(II)-ligand complexes in our experiments by combining Visual MINTEQ calculations of speciation and stability constants with experimental results from Fe(II) oxidation peaks. Using MINTEQ calculations, we first chose specific experimental parameters (ligand concentration, pH, E_H^{MEO}) where our targeted Fe(II)−ligand complex would be both redox-active (i.e., oxidizable) and present as the abundant species (i.e., our stability constants are thermodynamic as opposed to conditional, Supporting Information Section S4). Following triplicate Fe(II) additions into the cell, the first Fe(II) oxidation peak only was analyzed for $q_{(Fe^{II})}$, as any Fe(III) generated upon oxidation from the first peak alters the reduction potentials inside the cell (Supporting Information Section S11).[45] Reduction potentials for each Fe^{III}−L/Fe^{II}−L complex were obtained from integrating the current response of peaks using eq 2 above and calculation via the Nernst equation (see Supporting Information Section S11 for sample calculation). Integration of the peaks yielded $q_{(Fe^{II})}$, provided the ratio of Fe^{III}−L to Fe^{II}−L (%), which was then used in the Nernst equation to calculate E_H^{Φ}:

$$E_H = E_H^{\phi} - \frac{RT}{F}\ln\frac{\{Fe^{II}\}}{\{Fe^{III}\}} \quad (3)$$

where (E_H^{Φ}) (volts) is the apparent standard reduction potential of the redox couple under our solution conditions, which includes ligand complexation at a given pH. R(J/(mol K)) is the universal gas constant, T(K) is the absolute temperature, F is the Faraday constant (96,485 C/mol), and $\{Fe^{II}\}$ and $\{Fe^{III}\}$ denote activity, respectively. We assumed $q_{(Fe^{II})}$ was equivalent to moles of Fe(III) generated upon the oxidation of Fe(II).

RESULTS AND DISCUSSION

Profiling Fe(II) Oxidation Extent. The extent of Fe(II) oxidation was measured in the absence and presence of citrate and NTA across multiple E_H^{MEO} and pH, thus manipulating Fe(II) oxidation over fixed thermodynamic conditions (Figure 2a). Figure 2 shows $q_{(Fe^{II})}$ profiled across a range of E_H^{MEO}, +0.3 to +0.77 V at pH 4 (Figure 2b), and +0.1 to +0.3 V at pH 7 (Figure 2c), as well as a range of pH, 4−8, at a fixed E_H^{MEO} (+0.3 V) (Figure 2d). Trends show that an increase in $q_{(Fe^{II})}$ occurs when moving from a less-positive to a more-positive oxidizing potential, E_H^{MEO} (i.e. $\Delta G \ll 0$, Figure 2a), regardless of whether or not Fe(II) existed as a hexa-aquo species $[Fe(H_2O)_6^{2+}]$ or was complexed by other ligands [e.g. $Fe(H_2O)_5(OH)^+$, $Fe(H_2O)_3(Cit)^-$]. This trend exists because oxidation becomes more favorable as E_H^{MEO} increases toward or above the half-potentials of the Fe^{III}/Fe^{II}−L redox couples. The exception to this was experiments with ferrozine (Fz), where $q_{(Fe^{II})}$ remained zero at all conditions tested (Figure 2b−d). A lack of $Fe(Fz)_3^{4-}$ oxidation at various E_H^{MEO} was anticipated because nitrogen donor groups on ferrozine and other bipyridyl compounds stabilize Fe(II) through its low spin electron configuration.[19,34,35,48,49] The resulting redox potential of the low spin ferrozine complex is much higher than Fe^{III}/Fe^{II} (E_H = 0.97 V at pH 5, Figure 1c), which makes Fe(II) oxidation thermodynamically unfavorable.[48,49] Increasing pH also increased $q_{(Fe^{II})}$ (Figure 2d), for both $Fe(H_2O)_6^{2+}$ species and complexes with citrate and NTA [e.g., $Fe(H_2O)_3(cit)^-$, $Fe(NTA)_2^{4-}$]. At pH 7, under our experimental conditions [total Fe(II) concentration = 30 μM], $Fe(H_2O)_6^{2+}$ is stable only over a lower E_H range (E_H < +0.3 V) and therefore is readily oxidized in the absence of ligands at applied redox potentials within ± 120 mV of + 0.3 V (Supporting Information Section S12).[50,51] Additionally, hydroxide (mono and di) plays an important role in Fe(II) oxidation at higher pH[51] as the complexes $[Fe(H_2O)_5(OH)^+$, $Fe(H_2O)_4(OH)_2]$ possess redox potentials as low or lower than many organic ligands [e.g., $Fe(H_2O)_4(OH)_2$ = −0.1 V] that promote rapid oxidation.[14,19,51]

Differences between ligands were apparent, where at pH 4, $q_{(Fe^{II})}$was larger in NTA experiments than citrate at potentials from +0.3 up to +0.61 V (Figure 2b). This indicates that $Fe(H_2O)_2(NTA)^-$ was more reactive relative to $Fe(H_2O)_3(Cit)^-$ or $Fe(H_2O)_3(HCit)$ across these E_H^{MEO} and correlates well to what would be expected from lower redox potentials for Fe^{III}/Fe^{II} ligand complexes with NTA (+0.31 V vs SHE for $Fe(H_2O)_2(NTA)^-$) vs citrate (+0.33 V for $Fe(H_2O)_3(Cit)^-$) (Supporting Information Section S13).[15,19] Further, previous literature shows that NTA more strongly stabilizes Fe(III) than Fe(II) with respect to citrate.[15,19,52,53] Increasing pH from 4 to 6 opens up available binding spots in both citrate and NTA, assuring more complete oxidation of Fe(II) species as these ligands become increasingly deprotonated and more able to complex Fe(II). This effect is noticeable even at lower E_H^{MEO} (+0.3 V), where the higher degree of Fe(II) binding on citrate and NTA at higher pH leads to larger $q_{(Fe^{II})}$ than $Fe(H_2O)_6^{2+}$ alone (Figure 2d).

We decided to further investigate $q_{Fe(II)}$ at lower E_H^{MEO} and pH 7 since many natural waters are close to circumneutral (Figure 2c). Fe(II) in the absence of organic ligands is readily oxidized at this pH even at potentials as low as +0.15 V (Figure

https://doi.org/10.1021/acs.est.2c01782
Environ. Sci. Technol. 2022, 56, 9123−9132

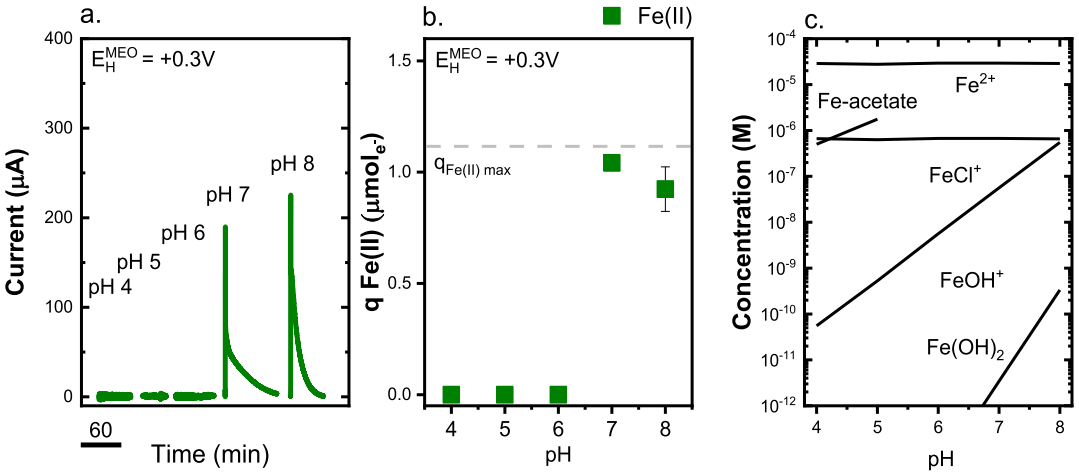

Figure 3. Fe(II) oxidation profiled across pH 4−8 at E_H^{MEO} = +0.30 V. (a) Current response for Fe(II) oxidation from pH 4−8 at E_H^{MEO} = +0.30 V. (b) $q_{Fe(II)}$ from pH 4−8 at E_H^{MEO} = +0.30 V. $q_{(Fe^{II})max}$ = the maximum number of electrons of Fe(II) to be donated if every mole of Fe(II) in the electrochemical cell (1.1 μmole e−) was oxidized c. Speciation of Fe(II) species present in the experimental parameters tested from pH 4−8 in the absence of other organic ligands (acetate excepted as it was used as a buffer). Note that weak Fe-acetate complexes were only present in abundance at pH 4 and 5.

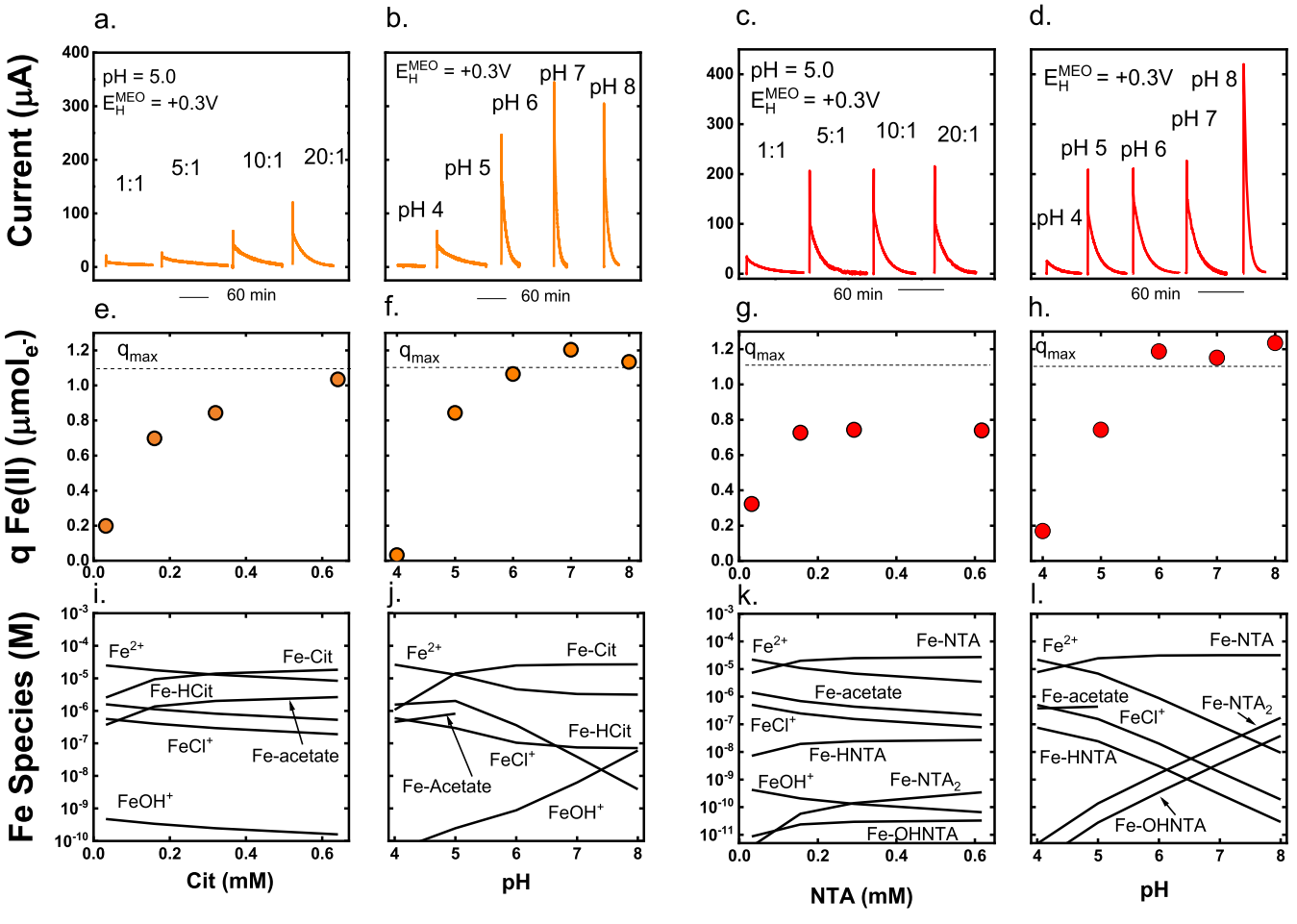

Figure 4. Fe(II) oxidation experiments in the presence of citrate and NTA at various ligand-to-iron ratios and across different pH values. Experiments using different ligand-to-iron ratios were performed at pH 5.0 in 10 mM acetate buffer with fixed $FeCl_2$ concentrations of 30 μM with ligand concentrations of approximately 30, 150, 300, and 600 μM (equating to roughly 1:1, 5:1, 10:1, and 20:1 ratios). Experiments ranging from pH 4−8 were all performed at 10:1 ligand-to-iron ratios. (a−d) Current responses for peaks across all experimental conditions. All experiments were performed at E_H^{MEO} = +0.3 V, as this potential was close to reported redox potentials of both Fe−L complexes. (e−h) Reported $q_{(Fe^{II})}$ for MEO experiments across all experimental conditions. The dotted lines correspond to the expected maximum q values assuming complete oxidation of Fe(II) on a per mole basis. (i−l) Speciation modeling of Fe-Citrate and Fe-NTA complexes at pH 5 and across different pH values.

https://doi.org/10.1021/acs.est.2c01782
Environ. Sci. Technol. 2022, 56, 9123−9132

2c). This is not surprising due to the presence of hydroxide complexes [e.g., $Fe(H_2O)_5(OH)^+$ as well as polymeric species], which are strong π donor ligands that enhance Fe^{II} oxidative reactivity (Figure 3c). NTA produced a smaller $q_{(Fe^{II})}$ than Fe(II) alone when oxidized at +0.15 and +0.2 V (Figure 2c). Because carboxyl ligating groups in NTA have smaller π donating effects than hydroxide, the higher (i.e., more positive) redox potentials of Fe(II) measured in our NTA experiments relative to $[Fe(H_2O)_5(OH)]^+$ at pH 7 indicate that the Fe(II) speciation in our NTA experiments was $Fe(NTA)_2^{4-}$, as the presence of a hydroxide ligand with NTA would likely enhance reactivity beyond $Fe(H_2O)_5(OH)^+$ alone.[19] 2:1 NTA to Fe complexes would bind Fe(II) with oxygen atoms in all six octahedral positions and prevent binding from strong hydroxide groups that form complexes with low E_H values.[15,19,32,33,52] Finally, citrate enabled $q_{(Fe^{II})}$ across all potentials at pH 7 (Figure 2c). The high reactivity of Fe(II) is surprising, if one assumes that all Fe(II) bound to citrate at pH 7 would be in the form of a 1:1 $Fe(H_2O)_3(Cit)^-$ complex ($E_H \approx +0.34$ V), but the presence of strong hydroxide ligands at pH 7 and the lability of citrate (i.e., weaker log$K$ compared to NTA) enhances the reactivity of Fe(II) through π donor effects with OH^-.[19] Several studies of Fe-citrate complexes have either suggested or shown the formation of strong complexes influenced by hydroxide, including ternary binuclear complexes resulting in lower than anticipated E_H values for ($[Fe_2(OH)_2Cit]$).[53−55] Under our experimental conditions, formation of these Fe(III) complexes would be likely upon Fe(II) oxidation given the circumneutral pH and excess ligand added. Additionally, rapid formation of Fe^{III}-hydroxides upon oxidation are possible due to the weaker stability of Fe^{III}-citrate complexes compared to NTA, which could promote heterogenous Fe(II) oxidation.[4,50,56] While precipitation of Fe^{III}-hydroxides is possible in both the absence and presence of citrate and NTA at pH 7 and 8 due to supersaturated conditions with respect to Fe(III) (i.e., Visual Minteq saturation indices positive for all Fe^{III}-hydroxides in all pH 7 and 8 experiments), we did not observe precipitate formation and feel that this is unlikely due to the time frame of our experiments [e.g., Fe(II) current response from oxidation occurs within 60 min] and the lack of Fe^{III}-hydroxides present in the electrochemical cell at the onset of the experiment [i.e., Fe^{III}-hydroxides have to be formed first though oxidation of Fe(II)].

Effect of Speciation on Fe^{II} Oxidation. Variations in $q_{Fe(II)}$ can be explained by examining the effects of citrate and NTA on Fe(II) speciation. Using Visual Minteq, we predicted Fe(II) speciation conditions in the absence and presence of different concentrations of citrate and NTA and at different pHs and then linked these calculations directly to experimental data where we directly manipulated ligand-to-iron ratios and pH (Figures 3 and 4).

Oxidation experiments in the absence of any organic ligands were performed from pH 4−8 at E_H^{MEO} = +0.3 V in order to model the effect of inorganic ligands (i.e., hydroxide species) on Fe(II) oxidation current response. From pH 4−6, no current was generated at E_H^{MEO} = +0.3 V (Figure 3a), indicating that the dominant species present was $Fe(H_2O)_6^{2+}$. This matched speciation modeling (Figure 3c), which resulted in no electrons being donated (Figure 3b). At pH 7, a sharp current response was observed, indicating an increase in Fe(II) reactivity at E_H^{MEO} = +0.3 V (Figure 3a) and $q_{(Fe^{II})}$ (Figure 3b). Speciation modeling at pH 7 showed nM concentrations of $Fe(H_2O)_5(OH)^+$ (Table S7), which would greatly influence Fe(II) oxidation as stated earlier (Supporting Information Section S14). A sharper response was visible at pH 8 (Figure 3a), which corresponded to higher concentrations of $Fe(H_2O)_5(OH)^+$ (∼550 nM, Table S7) based on our speciation modeling.

For citrate, $Fe(H_2O)_3(Cit)^-$ and $Fe(H_2O)_3(HCit)$ are the two main complexes expected to be in abundance under varying solution conditions (Figure 4i,j). At pH 5, $Fe(H_2O)_3(Cit)^-$ is important relative to $Fe(H_2O)_6^{2+}$ only at ligand-to-iron ratios greater than 10:1 (Figure 4i). Across a pH range from 4 to 8, $Fe(H_2O)_3(Cit)^-$ dominates as the main complex at or above pH 5 (Figure 4j). Although speciation of $Fe(H_2O)_3(Cit)^-$ and $Fe(H_2O)_3(HCit)$ varies across solution conditions in both cases, a visual comparison of current peaks and experimental data with trends in Fe(II) speciation suggests a parallel between $q_{(Fe^{II})}$ and Fe-Cit species (Figure 4e,f). This suggests that $Fe(H_2O)_3(Cit)^-$ is the main complex responsible for Fe(II) reactivity (oxidation) across most experimental parameters, although $Fe(H_2O)_3(HCit)$ may contribute to $q_{(Fe^{II})}$at higher ligand-to-Fe(II) ratios at pH 5 (Figure 4e). Increased q values at higher pH in the absence of $Fe(H_2O)_3(HCit)$ correlate with the appearance of OH^- and indicate its influence as a ligand for Fe(II) (Figure 4b,f,j) as stated previously.[57−59] This is more likely with citrate than NTA because of the liability of citrate only occupying 3 out of 6 octahedral coordination positions of Fe(II), as opposed to NTA or NTA_2, which can occupy 4 and 6.[52]

Additionally, qualitative analysis of current generated from Fe(II) oxidation shows an increase in peak size, corresponding to a reported increase in $q_{(Fe^{II})}$ (Figure 4e,f) with citrate concentration and pH (Figure 3a,b). While we did not analyze current response in this study for oxidation kinetics, it is interesting to note that peak heights increase with increasing ligand concentration and pH, that is, peaks became sharper with less tailing. This likely indicates changes in Fe(II) oxidation kinetics that are parallel with these increasing experimental parameters (particularly pH), which would match previous work looking at Fe^{II}-citrate oxidation kinetics.[15,22,57−59]

For NTA, our modeling showed that the most predominant complex present across solution conditions was a mono $Fe(H_2O)_2(NTA)^-$ complex, with bis $Fe(NTA)_2^{4-}$ complexes appearing at pH 7 and increasing in abundance at pH 8 (Figure 4k,l). Unlike citrate, the 1−1 $Fe(H_2O)_2(NTA)^-$ complex prevailed over free Fe(II) at lower ligand-to-iron ratios (Figure 4k). While citrate and NTA are both tricarboxylic acids, the nitrogen in NTA increases the ligand stability and allows NTA to occupy four coordination positions on Fe(II) in a 1 to 1 $Fe(H_2O)_2(NTA)^-$ complex as opposed to three for citrate.[52] This is reflected in its higher stability constant (log $K_{Fe(II)}$ = 10.18) than citrate (log $K_{Fe(II)}$ = 5.89) (Table S2). A comparison of experimental data with trends in Fe^{II}−NTA speciation suggests a parallel between $q_{(Fe^{II})}$ and $Fe(H_2O)_2(NTA)^-$ (Figure 4g,h). Fe(II) oxidation extent and current peaks associated with NTA experiments do not increase with increasing NTA concentration (Figure 4c,g), as it does in the case with citrate (Figure 4e), which is due to the 1−1 $Fe(H_2O)_2(NTA)^-$ complex being the only abundant complex present in all solution conditions. While increasing pH increased $q_{Fe(II)}$ and oxidation peak sizes in our NTA experiments (Figure 4d,h), our modeling shows that peak size increases are due to the formation of reactive $Fe(NTA)_2^{4-}$

https://doi.org/10.1021/acs.est.2c01782
Environ. Sci. Technol. 2022, 56, 9123−9132

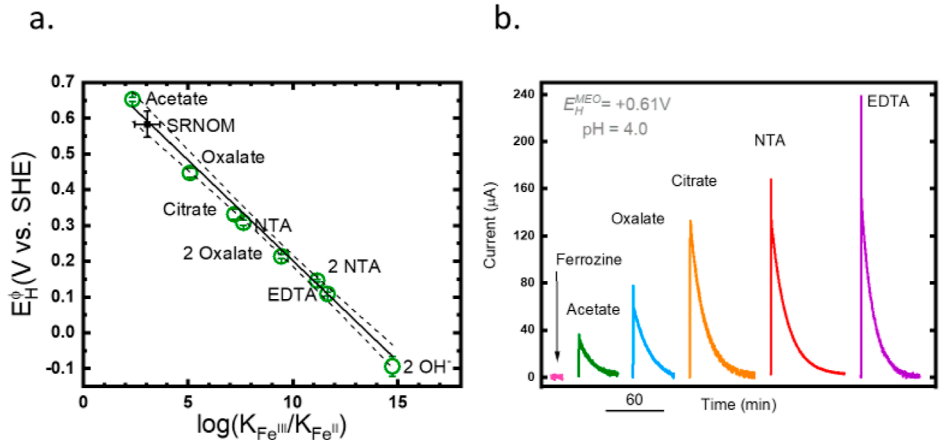

Figure 5. Relationships between experimental data obtained and reduction potentials measured for individual ligand complexes. (a) Nernstian relationship between experimental E_H^ϕ and known stability constants of model ligands (green circles). Some error bars are small and hidden within the plotted points. Solid and dotted lines represent the linear regression through the data and the 95% confidence interval, respectively. The fit yielded a slope of −0.056 ± 0.002, a *y*-intercept of +0.76 ± 0.02, and r^2 = 0.99. Fe-SRNOM log*K* values at pH 4 were experimentally derived using the Nernstian relationship and plotted (black square). (b) Current response derived from E_H^{MEO} experiments at +0.61 V, pH 4 with six ligands. Increases in peak response correlate with calculated reduction potentials of Fe−L complexes.

complexes (log*K* = 12.62) with increasing pH, which differs from citrate experiments at higher pH, where modeling confirmed an influence from OH^- ligands (Figure 4j). 2−1 NTA complexes coordinate Fe(II) in all six positions with oxygen donor atoms thereby preventing interaction with OH^-, which increases Fe(II) oxidation.[22,60]

Relationship between Experimentally Derived Redox Potentials and Stability Constants. We used our data to develop a correlation between the redox potentials of iron-ligand complexes and the thermodynamic stability constants of the complexes based upon the Nernst equation. Measurements of $q_{(Fe^{II})}$indicate the ratio (%) of Fe(II) initially added to the cell that was oxidized to Fe(III). Quantifying the ratio of Fe(II) and Fe(III) in our system enables us to calculate E_H^ϕ using eq 3 above (Supporting Information Section S11). Our measured redox potentials correlated with previously reported redox potentials in the literature (Table S6).[13,15,19] Figure 5a shows that redox potentials obtained experimentally for multiple complexes were linearly correlated with the ratio between Fe(III) logK_{Therm} and Fe(II) logK_{Therm}. This indicates that ligands that are more strongly inclined to complex Fe(III) with respect to Fe(II) decrease the E_H of the Fe^{III}/Fe^{II} couple, which matches previous studies that have found the same relationship using probe compound reduction kinetics.[15,17,18,22] Our correlation shows that the effect of ligands on Fe(II) and Fe(III) potentials is approximately Nernstian with a slope of −0.056 ± 0.002, which is not significantly different from the theoretical slope of −0.059 for a one electron transfer; thus, any kinetic effects are minimal.[61] The *y*-intercept, +0.76 ± 0.02, also corresponds to the standard one electron reduction potential of the Fe^{III}/Fe^{II} couple (+0.77 V). Experimentally determined potentials were primarily at the lower pH values (5) or at explicitly chosen conditions (i.e., E_H, pH, ligand-to-iron ratio) to capture thermodynamic stability constants. Further, measured redox potentials of iron complexes with highly labile ligands, such as oxalate and citrate, are easily influenced by side reactions involving hydroxide ligands, which preclude their measurement at high pH,[19] while weaker 1:1 complexes tend to have higher potentials, bis-oxalate and bis-NTA were among two of the strongest Fe(II)-ligand organic complexes with lower potentials in our experiments. Stronger bonding from more π donor ligands enhances metal basicity, which forces Fe(II) to donate its electron thereby stabilizing Fe(III).[49] This effect may be analogous to Fe(II) complexation in the aquatic environment, where 2−1 or 3−1 complexes are formed with oxalate or other low molecular weight carboxylic acids when ligands (e.g., those present in DOM) exist in excess of Fe(II).[62]

We used our linear relationship to predict the ratio of unknown stability constants of iron with an aquatic DOM isolate, Suwannee River Natural Organic Matter at pH 4. We chose pH 4 to capture the binding behavior of carboxylic (Type-A) functionalities based on DOM acid-base titration data[62−65] and humic binding models developed by Tipping et al.[62,63] The experimental E_H^ϕ value for the SRNOM-complexed Fe^{III}/Fe^{II} couple was +0.583 ± 0.036 V, which correspondingly yielded a $\log(K_{Fe(III)}/K_{Fe(II)})$ value of 3.06 ± 0.60. This value is similar to other iron-humic or iron-fulvic acid values in the literature[62,63] and indicates that the ligand sites responsible for Fe(II) binding at pH 4 are weak in nature and similar to acetate in binding strength. Additionally, the data indicates that in the presence of SRNOM at pH 4, Fe(II) oxidation extent is increased only very modestly (slightly more than acetate). Our observation suggests that Fe^{II}-SRNOM is a weak reductant at this pH.[15,66,67] We are currently using the generated relationship to work with other fulvic and humic acid standards as well as from a variety of surface water DOM collected globally to elucidate their stability constants.

Previous work utilizing MEA to investigate the reducibility of solid-phase Fe^{III}-species were able to link reduction kinetics pseudo-first order rate constants from current response [i.e., k_{obs} (s^{-1})] in addition to the amount of Fe(III) reduced (q_{tot}^{Fe3+}, extent) obtained by peak integration.[45] While our study did not attempt to fit current kinetics from oxidation peaks in a similar manner, it is interesting to note that a qualitative relationship between peak height and redox potential was observed at low pH (Figure 5b) with Fe(II)-ligand species and with increasing pH (Figures 3a and 4b,d). Good correlations between potentials of iron-ligand redox couples obtained in our experiments versus calculated potentials and potentials in the literature (Table S6) indicates that electron transfer obeys Marcus theory (eq 4)

https://doi.org/10.1021/acs.est.2c01782
Environ. Sci. Technol. 2022, 56, 9123−9132

$$\alpha = \frac{1}{2} + \frac{F(E - E^{\circ})}{2\lambda} \quad (4)$$

where α is the transfer coefficient, E is the potential (V) of complexes found in our experiment, E° is the potential (V) of complexes reported in the literature at standard conditions, F is the Faraday constant, and λ (J mol^{-1}) represents the reorganization energy associated with the electron transfer from the Fe^{II}−L complex to the oxidized mediator.[19,68] Due to the good agreement between expected and measured potentials (Table S6), the maximum value of the transfer coefficient term, α, was estimated to be 0.512 from the t_{2g} to e_g absorption peak (or λ) of $Fe(H_2O)_6^{2+}$ (1000 nm or 119, 640 J mol^{-1}, Supporting Information Section S15)[19] and the maximum ΔE of 0.03 V for $Fe(NTA)_2$ from Table S6. All other Fe(II) absorption peaks are higher energy indicating that the second term approaches 0 and that α is close to 0.5 (Figure S6, Supporting Information Section S15). An α value of 0.5 is a typical value that indicates the measure of symmetry of the energy barrier at the electrode;[68] in our case, the α value indicates small internal reorganization (λ) of the Fe(II)− complex upon oxidation by the oxidized mediator species, which is suggestive of an outer sphere electron transfer.[19,68]

Environmental Implications. This work provides the first direct experimental evidence of the effect of organic ligands on the extent of Fe(II) oxidation under constrained E_H and pH conditions. We were able to directly measure E_H^{ϕ} of our target complexes, corroborating previous studies[13−15,17,18,22,26,28] that indirectly link calculated redox potentials of Fe complexes to the reduction kinetics of probe compounds. Our approach enables us to both measure the effects of ligands on iron redox reactions and determine the relative strengths of the Fe(II) to Fe(III) complexes.

Our findings in this study have a few important implications. First, our work highlights the flexible capability of ligands to be able to effect Fe(II) reactivity across a range of thermodynamic conditions, including those conditions which are known to stabilize Fe(II) against abiotic oxidation (i.e., low E_H, pH).[4,38] Depending on the E_H of the electron acceptor, certain ligands may promote or enhance abiotic electron transfer under these unfavorable circumstances, which enables abiotic Fe(II) oxidation to outcompete biologically mediated Fe(II) oxidation.[36,37] Additionally, we show that some Fe(III)-stabilizing chelates, such as NTA, may stabilize Fe(II) species against abiotic oxidation at higher pH higher due to the inhibition of hydroxide ligands from forming complexes with Fe(II) (Figure 2c). These processes along with reduced moieties in DOM[22] may play an important role in stabilizing Fe(II) in (sub)oxic environments at circumneutral pH.[69,70]

Further, we were able to accurately measure the E_H^{Φ} of complexes from our experimental data, to build a Nernstian relationship that directly correlated E_H^{Φ} to stability constant ratios of several model ligands. This relationship spans a large range of redox potentials and stability constant ratios and allows us to use this scale to estimate stability constant ratios of other unknown ligands, especially those associated with DOM.[71] We anticipate the use of MEA in the future to help us better understand redox processes in the environment, particularly iron redox systems such as iron adsorbed to mineral surfaces or Fe^{III} complexed to DOM. Thus, MEA has the potential to help us better understand the role that iron plays in many important biogeochemical and environmental reactions ranging from greenhouse gas emissions to the remediation of redox sensitive contaminants.

■ ASSOCIATED CONTENT

Supporting Information

The Supporting Information is available free of charge at https://pubs.acs.org/doi/10.1021/acs.est.2c01782.

Chemicals used in the study, choice of mediators used, examples of speciation calculation using Visual Minteq, examples of experimental parameters chosen using speciation data, calculation of stability constants, stability constants generated in Visual Minteq, list of calculated stability constants in our experiments, calculation of redox potential from stability constants, potentiometry of the iron ferrozine complex, calculation of thermodynamic stability constants for iron ferrozine complex, apparent reduction potential calculations, calculated redox potentials of the Fe^{III}/Fe^{II} redox couple, comparison of experimental redox potentials vs literature redox potentials, Fe(II) speciation calculations from pH 4−8 in Visual Minteq, and Marcus expression (PDF)

■ AUTHOR INFORMATION

Corresponding Authors

Jeffrey M. Hudson − *Department of Civil & Environmental Engineering, University of Delaware, Newark, Delaware 19716, United States*; Email: hudsonjm@udel.edu

Yu-Ping Chin − *Department of Civil & Environmental Engineering, University of Delaware, Newark, Delaware 19716, United States*; orcid.org/0000-0003-1427-9156; Email: yochin@udel.edu

Author

George W. Luther, III − *School of Marine Science and Policy, University of Delaware, Lewes, Delaware 19958, United States*

Complete contact information is available at: https://pubs.acs.org/10.1021/acs.est.2c01782

Notes

The authors declare no competing financial interest.

■ ACKNOWLEDGMENTS

We like to thank Dr. Pei Chiu (University of Delaware) and Dr. Brandon McAdams (NETL) for fruitful discussions and Anthony Sigman-Lowery for assisting in the measurements. This work was supported by a United States Department of Energy (DOE) Oak Ridge Institute for Science and Education (ORISE) Science Graduate Student Research Fellowship awarded to J.H. and by the National Science Foundation (NSF) Grant EAR-2029665 (Y.C.).

■ REFERENCES

(1) Cornell, R. M.; Schwertmann, U. *The Iron Oxides: Structure, Properties, Reactions, Occurrences, and Uses*; Wiley-vch: Weinheim, 2003; Vol. 2, p 71.

(2) Morel, F. M.; Hering, J. G. *Principles and Applications of Aquatic Chemistry*; John Wiley & Sons, 1993; pp 466−477.

(3) Stumm, W.; Morgan, J. J.. *Aquatic Chemistry: Chemical Equilibria and Rates in Natural Waters*; John Wiley & Sons, 2012; Vol. *126*, p 455.

(4) Kappler, A.; Straub, K. L. Geomicrobiological cycling of iron. *Rev. Mineral. Geochem.* **2005**, *59*, 85−108.

(5) Theis, T. L.; Singer, P. C. Complexation of iron(II) by organic matter and its effect on iron(II) oxidation. *Environ. Sci. Technol.* **1974**, *8*, 569−573.
(6) Hofstetter, T. B.; Heijman, C. G.; Haderlein, S. B.; Holliger, C.; Schwarzenbach, R. P. Complete reduction of TNT and other (poly) nitroaromatic compounds under iron-reducing subsurface conditions. *Environ. Sci. Technol.* **1999**, *33*, 1479−1487.
(7) Schwarzenbach, R. P., Gschwend, P. M.; Imboden, D. M. *Environmental Organic Chemistry*; John Wiley & Sons, 2005; p 555.
(8) Jones, M. E.; LaCroix, R. E.; Zeigler, J.; Ying, S. C.; Nico, P. S.; Keiluweit, M. Enzymes, manganese, or iron? Drivers of oxidative organic matter decomposition in soils. *Environ. Sci. Technol.* **2020**, *54*, 14114−14123.
(9) Taillefert, M.; Bono, A. B.; Luther, G. W. Reactivity of freshly formed Fe (III) in synthetic solutions and (pore) waters: voltammetric evidence of an aging process. *Environ. Sci. Technol.* **2000**, *34*, 2169−2177.
(10) Taillefert, M.; Hover, V. C.; Rozan, T. F.; Theberge, S. M.; Luther, G. W. The influence of sulfides on soluble organic-Fe (III) in anoxic sediment porewaters. *Estuaries* **2002**, *25*, 1088−1096.
(11) Klar, J. K.; Homoky, W. B.; Statham, P. J.; Birchill, A. J.; Harris, E. L.; Woodward, E. M. S.; Silburn, B.; Cooper, M. J.; James, R. H.; Connelly, D. P.; Chever, F.; Lichtschlag, A.; Graves, C. Stability of dissolved and soluble Fe (II) in shelf sediment pore waters and release to an oxic water column. *Biogeochemistry* **2017**, *135*, 49−67.
(12) Tamura, H.; Goto, K.; Nagayama, M. Effect of anions on the oxygenation of ferrous ion in neutral solutions. *J. Inorg. Nucl. Chem.* **1976**, *38*, 113−117.
(13) Strathmann, T. J. Redox reactivity of organically complexed iron (II) species with aquatic contaminants. *Aquatic Redox Chemistry*; American Chemical Society, 2011; pp 283−313.
(14) Strathmann, T. J.; Stone, A. T. Reduction of the pesticides oxamyl and methomyl by FeII: effect of pH and inorganic ligands. *Environ. Sci. Technol.* **2002**, *36*, 653−661.
(15) Buerge, I. J.; Hug, S. J. Influence of organic ligands on chromium (VI) reduction by iron (II). *Environ. Sci. Technol.* **1998**, *32*, 2092−2099.
(16) Rose, A. L.; Waite, T. D. Effect of dissolved natural organic matter on the kinetics of ferrous iron oxygenation in seawater. *Environ. Sci. Technol.* **2003**, *37*, 4877−4886.
(17) Naka, D.; Kim, D.; Strathmann, T. J. Abiotic reduction of nitroaromatic compounds by aqueous iron (II)− catechol complexes. *Environ. Sci. Technol.* **2006**, *40*, 3006−3012.
(18) Naka, D.; Kim, D.; Carbonaro, R. F.; Strathmann, T. J. Abiotic reduction of nitroaromatic contaminants by iron (II) complexes with organothiol ligands. *Environ. Toxicol. Chem.* **2008**, *27*, 1257−1266.
(19) Luther, G. W., III *Inorganic Chemistry for Geochemistry and Environmental Sciences: Fundamentals and Applications*; John Wiley & Sons, 2016; p 237.
(20) Stumm, W.; Sulzberger, B. The cycling of iron in natural environments: considerations based on laboratory studies of heterogeneous redox processes. *Geochim. Cosmochim. Acta* **1992**, *56*, 3233−3257.
(21) Catrouillet, C.; Davranche, M.; Dia, A.; Bouhnik-Le Coz, M.; Marsac, R.; Pourret, O.; Gruau, G. Geochemical modeling of Fe (II) binding to humic and fulvic acids. *Chem. Geol.* **2014**, *372*, 109−118.
(22) Daugherty, E. E.; Gilbert, B.; Nico, P. S.; Borch, T. Complexation and redox buffering of iron (II) by dissolved organic matter. *Environ. Sci. Technol.* **2017**, *51*, 11096−11104.
(23) Fritzsche, A.; Bosch, J.; Sander, M.; Schröder, C.; Byrne, J. M.; Ritschel, T.; Joshi, P.; Maisch, M.; Meckenstock, R. U.; Kappler, A.; Totsche, K. U. Organic matter from redoximorphic soils accelerates and sustains microbial Fe (III) reduction. *Environ. Sci. Technol.* **2021**, *55*, 10821−10831.
(24) Curti, L.; Moore, O. W.; Babakhani, P.; Xiao, K. Q.; Woulds, C.; Bray, A. W.; Fisher, B. J.; Kazemian, M.; Kaulich, B.; Peacock, C. L. Carboxyl-richness controls organic carbon preservation during coprecipitation with iron (oxyhydr) oxides in the natural environment. *Commun. Earth Environ.* **2021**, *2*, 1−13.
(25) Kim, D.; Duckworth, O. W.; Strathmann, T. J. Hydroxamate siderophore-promoted reactions between iron (II) and nitroaromatic groundwater contaminants. *Geochim. Cosmochim. Acta* **2009**, *73*, 1297−1311.
(26) Duckworth, O. W.; Sposito, G. Siderophore− manganese (III) interactions. I. Air-oxidation of manganese (II) promoted by desferrioxamine B. *Environ. Sci. Technol.* **2005**, *39*, 6037−6044.
(27) Rush, J.; Koppenol, W. H. The reaction between ferrous polyaminocarboxylate complexes and hydrogen peroxide: An investigation of the reaction intermediates by stopped flow spectrophotometry. *J. Inorg. Biochem.* **1987**, *29*, 199−215.
(28) Joe-Wong, C.; Shoenfelt, E.; Hauser, E. J.; Crompton, N.; Myneni, S. C. B. Estimation of reactive thiol concentrations in dissolved organic matter and bacterial cell membranes in aquatic systems. *Environ. Sci. Technol.* **2012**, *46*, 9854−9861.
(29) Strathmann, T. J.; Stone, A. T. Reduction of oxamyl and related pesticides by FeII: influence of organic ligands and natural organic matter. *Environ. Sci. Technol.* **2002**, *36*, 5172−5183.
(30) Yu, H.; Zhang, P.; Liu, J.; Zheng, Y.; Mustapha, N. A. Effects of low-molecular-weight organic acids/thiols on hydroxyl radical production from natural siderite oxidation. *Chem. Geol.* **2021**, *584*, 120537.
(31) Batinić-Haberle, I.; Spasojević, I.; Hambright, P.; Benov, L.; Crumbliss, A. L.; Fridovich, I. Relationship among redox potentials, proton dissociation constants of pyrrolic nitrogens, and in vivo and in vitro superoxide dismutating activities of manganese (III) and iron (III) water-soluble porphyrins. *Inorg. Chem.* **1999**, *38*, 4011−4022.
(32) Sada, E.; Kumazawa, H.; Machida, H. Oxidation kinetics of FeII-EDTA and FeII-NTA chelates by dissolved oxygen. *Ind. Eng. Chem. Res.* **1987**, *26*, 1468−1472.
(33) Seibig, S.; van Eldik, R. Kinetics of [FeII (edta)] oxidation by molecular oxygen revisited. New evidence for a multistep mechanism. *Inorg. Chem.* **1997**, *36*, 4115−4120.
(34) Thompsen, J. C.; Mottola, H. A. Kinetics of the complexation of iron (II) with ferrozine. *Anal. Chem.* **1984**, *56*, 755−757.
(35) Viollier, E.; Inglett, P. W.; Hunter, K.; Roychoudhury, A. N.; Van Cappellen, P. The ferrozine method revisited: Fe (II)/Fe (III) determination in natural waters. *Appl. Geochem.* **2000**, *15*, 785−790.
(36) Kopf, S. H.; Henny, C.; Newman, D. K. Ligand-enhanced abiotic iron oxidation and the effects of chemical versus biological iron cycling in anoxic environments. *Environ. Sci. Technol.* **2013**, *47*, 2602−2611.
(37) Peng, C.; Bryce, C.; Sundman, A.; Borch, T.; Kappler, A. Organic matter complexation promotes Fe (II) oxidation by the photoautotrophic Fe (II)-oxidizer Rhodopseudomonas palustris TIE-1. *ACS Earth Space Chem.* **2019**, *3*, 531−536.
(38) Huang, J.; Jones, A.; Waite, T. D.; Chen, Y.; Huang, X.; Rosso, K. M.; Kappler, A.; Mansor, M.; Tratnyek, P. G.; Zhang, H. Fe (II) redox chemistry in the environment. *Chem. Rev.* **2021**, *121*, 8161−8233.
(39) Kappler, A.; Bryce, C.; Mansor, M.; Lueder, U.; Byrne, J. M.; Swanner, E. D. An evolving view on biogeochemical cycling of iron. *Nat. Rev. Microbiol.* **2021**, *19*, 360−374.
(40) Miller, C. J.; Lee, S. M. V.; Rose, A. L.; Waite, T. D. Impact of natural organic matter on H2O2-mediated oxidation of Fe (II) in coastal seawaters. *Environ. Sci. Technol.* **2012**, *46*, 11078−11085.
(41) Klüpfel, L.; Piepenbrock, A.; Kappler, A.; Sander, M. Humic substances as fully regenerable electron acceptors in recurrently anoxic environments. *Nat. Geosci.* **2014**, *7*, 195−200.
(42) Aeschbacher, M.; Sander, M.; Schwarzenbach, R. P. Novel electrochemical approach to assess the redox properties of humic substances. *Environ. Sci. Technol.* **2010**, *44*, 87−93.
(43) Gorski, C. A.; Aeschbacher, M.; Soltermann, D.; Voegelin, A.; Baeyens, B.; Marques Fernandes, M.; Hofstetter, T. B.; Sander, M. Redox properties of structural Fe in clay minerals. 1. Electrochemical quantification of electron-donating and-accepting capacities of smectites. *Environ. Sci. Technol.* **2012**, *46*, 9360−9368.

https://doi.org/10.1021/acs.est.2c01782
Environ. Sci. Technol. 2022, 56, 9123−9132

(44) Sander, M.; Hofstetter, T. B.; Gorski, C. A. Electrochemical analyses of redox-active iron minerals: a review of nonmediated and mediated approaches. *Environ. Sci. Technol.* **2015**, *49*, 5862−5878.
(45) Aeppli, M.; Voegelin, A.; Gorski, C. A.; Hofstetter, T. B.; Sander, M. Mediated electrochemical reduction of iron (oxyhydr-) oxides under defined thermodynamic boundary conditions. *Environ. Sci. Technol.* **2018**, *52*, 560−570.
(46) Gorski, C. A.; Klüpfel, L.; Voegelin, A.; Sander, M.; Hofstetter, T. B. Redox properties of structural Fe in clay minerals. 2. Electrochemical and spectroscopic characterization of electron transfer irreversibility in ferruginous smectite, SWa-1. *Environ. Sci. Technol.* **2012**, *46*, 9369−9377.
(47) Gorski, C. A.; Klüpfel, L. E.; Voegelin, A.; Sander, M.; Hofstetter, T. B. Redox properties of structural Fe in clay minerals: 3. Relationships between smectite redox and structural properties. *Environ. Sci. Technol.* **2013**, *47*, 13477−13485.
(48) Stookey, L. L. Ferrozine—a new spectrophotometric reagent for iron. *Anal. Chem.* **1970**, *42*, 779−781.
(49) Luther, G. W., III; Kostka, J. E.; Church, T. M.; Sulzberger, B.; Stumm, W. Seasonal iron cycling in the salt-marsh sedimentary environment: the importance of ligand complexes with Fe (II) and Fe (III) in the dissolution of Fe (III) minerals and pyrite, respectively. *Mar. Chem.* **1992**, *40*, 81−103.
(50) Hem, J. D.; Cropper, W. H. *Chemistry of Iron in Natural Water*; USGS Water Supply Papers, 1962; Vol. *1459*; p 5.
(51) Santana-Casiano, J. M.; González-Dávila, M.; Millero, F. J. Oxidation of nanomolar levels of Fe(II) with oxygen in natural waters. *Environ. Sci. Technol.* **2005**, *39*, 2073−2079.
(52) Zhou, N., Luther, G. W.; Chan, C. S. *Ligand Effects on Biotic and Abiotic Fe (II) Oxidation by the Microaerophile Sideroxydans Lithotrophicus*; Environmental Science & Technology, 2021.
(53) Taillefert, M.; Beckler, J. S.; Carey, E.; Burns, J. L.; Fennessey, C. M.; DiChristina, T. J. Shewanella putrefaciens produces an Fe (III)-solubilizing organic ligand during anaerobic respiration on insoluble Fe (III) oxides. *J. Inorg. Biochem.* **2007**, *101*, 1760.
(54) Königsberger, L. C.; Königsberger, E.; May, P. M.; Hefter, G. T. Complexation of iron (III) and iron (II) by citrate. Implications for iron speciation in blood plasma. *J. Inorg. Biochem.* **2000**, *78*, 175−184.
(55) Hamada, Y. Z.; Bayakly, N.; Peipho, A.; Carlson, B. Accurate Potentiometric Studies of Chromium-Citrate and Ferric-Citrate Complexes in Aqueous Solutions at Physiological and Alkaline pH Values. *Synth. React. Inorg. Metal-Org. Nano-Metal Chem.* **2006**, *36*, 469−476.
(56) Gorski, C. A.; Edwards, R.; Sander, M.; Hofstetter, T. B.; Stewart, S. M. Thermodynamic characterization of iron oxide−aqueous Fe2+ redox couples. *Environ. Sci. Technol.* **2016**, *50*, 8538−8547.
(57) Pham, A. N.; Waite, T. D. Modeling the kinetics of Fe (II) oxidation in the presence of citrate and salicylate in aqueous solutions at pH 6.0− 8.0 and 25 C. *J. Phys. Chem. A* **2008**, *112*, 5395−5405.
(58) Pham, A. N.; Waite, T. D. Oxygenation of Fe (II) in the presence of citrate in aqueous solutions at pH 6.0− 8.0 and 25 C: Interpretation from an Fe (II)/citrate speciation perspective. *J. Phys. Chem. A* **2008**, *112*, 643−651.
(59) Jones, A. M.; Griffin, P. J.; Waite, T. D. Ferrous iron oxidation by molecular oxygen under acidic conditions: the effect of citrate, EDTA and fulvic acid. *Geochim. Cosmochim. Acta* **2015**, *160*, 117−131.
(60) González-Davila, M.; Santana-Casiano, J. M.; Millero, F. J. Oxidation of iron (II) nanomolar with H2O2 in seawater. *Geochim. Cosmochim. Acta* **2005**, *69*, 83−93.
(61) Taylor, S. W.; Luther, G. W.; Waite, J. H. Polarographic and spectrophotometric investigation of iron (III) complexation to 3, 4-dihydroxyphenylalanine-containing peptides and proteins from Mytilus edulis. *Inorg. Chem.* **1994**, *33*, 5819−5824.
(62) Tipping, E. *Cation Binding by Humic Substances*; Cambridge University Press, 2002; Vol. *12*; p 171.
(63) Tipping, E. Humic ion-binding model VI: an improved description of the interactions of protons and metal ions with humic substances. *Aquat. Geochem.* **1998**, *4*, 3−47.
(64) Perdue, E. M.; Lytle, C. R. A distribution model for binding of protons and metal ions by humic substances. *Environ. Sci. Technol.* **1983**, *17*, 654−660.
(65) Carbonaro, R. F.; Di Toro, D. M. Linear free energy relationships for metal−ligand complexation: Monodentate binding to negatively-charged oxygen donor atoms. *Geochem. Cosmochim. Acta* **2007**, *71*, 3958−3968.
(66) Hakala, J. A.; Chin, Y.-P.; Weber, E. J. Influence of dissolved organic matter and Fe (II) on the abiotic reduction of pentachloronitrobenzene. *Environ. Sci. Technol.* **2007**, *41*, 7337−7342.
(67) Hakala, J. A.; Fimmen, R. L.; Chin, Y.-P.; Agrawal, S. G.; Ward, C. P. Assessment of the geochemical reactivity of Fe-DOM complexes in wetland sediment pore waters using a nitroaromatic probe compound. *Geochim. Cosmochim. Acta* **2009**, *73*, 1382−1393.
(68) Bard, A. J.; Faulkner, L. R. Fundamentals and applications. *Electrochem. Methods* **2001**, *2*, 580−632.
(69) Klar, J. K.; Homoky, W. B.; Statham, P. J.; Birchill, A. J.; Harris, E. L.; Woodward, E. M. S.; Silburn, B.; Cooper, M. J.; James, R. H.; Connelly, D. P.; Chever, F.; Lichtschlag, A.; Graves, C. Stability of dissolved and soluble Fe (II) in shelf sediment pore waters and release to an oxic water column. *Biogeochemistry* **2017**, *135*, 49−67.
(70) Herrmann, A. J.; Sorwat, J.; Byrne, J. M.; Frankenberg-Dinkel, N.; Gehringer, M. M. Diurnal Fe (II)/Fe (III) cycling and enhanced O 2 production in a simulated Archean marine oxygen oasis. *Nat. Commun.* **2021**, *12*, 2069.
(71) Luther, G. W., III; Mullaugh, K. M.; Hauser, E. J.; Rader, K. J.; Di Toro, D. M. Determination of ambient dissolved metal ligand complexation parameters via kinetics and pseudo-voltammetry experiments. *Mar. Chem.* **2021**, *234*, 103998.

https://doi.org/10.1021/acs.est.2c01782
Environ. Sci. Technol. 2022, 56, 9123−9132